NASA-CR-202196

AN ELECTRON SENSOR FOR THE PULSATING AURORA II (PULSAUR II) MISSION

by

J.R. Sharber, J.R. Scherrer, R.A. Frahm, and B. Piepgrass
Southwest Research Institute
6220 Culebra Road
San Antonio, TX 78238-5166

Final Technical Report
NASA Grant NAG5-671
SwRI Project 15-3822

submitted to

Larry J. Early
NASA Technical Officer
Code 840
NASA Wallops Flight Facility
Wallops Island, VA 23337

March 31, 1996

TABLE OF CONTENTS

ABSTRACT 1

INTRODUCTION 1

PULSAUR LOW-ENERGY ELECTRON SPECTROMETER 2

HIGH VOLTAGE POWER SUPPLIES 6

CALIBRATION 6

THE PULSAUR II FLIGHT 18
- *Electron Spectrometer Data* 18
- *Instrument Performance* 21

PUBLICATIONS AND PRESENTATIONS 21

CONCLUDING COMMENTS 22

REFERENCES 22

AN ELECTRON SENSOR FOR THE PULSATING AURORA II (PULSAUR II) MISSION

ABSTRACT

The purpose of this grant was to provide a low-energy electron detector to be flown on the PULSAUR II rocket payload for investigation of the pulsating aurora. In the course of this grant, the instrument, a tophat analyzer, was built and calibrated by the combined efforts of Southwest Research Institute, Mullard Space Sciences Laboratory, Rutherford Appleton Laboratory, and Goddard Space Flight Center, and successfully flown into an active, early morning, pulsating aurora over Andoya, Norway, on February 9, 1994. This report provides a description of the instrument and its calibration and gives examples of data obtained on the flight.

INTRODUCTION

One of the most striking of the morningside auroral phenomena is the pulsating aurora. The pulsations in the auroral light generally have periods of ~1-20 seconds and are caused by modulation of the precipitating electron flux responsible for the emissions. Measurements from rocket instrumentation have usually found that the electrons being modulated are those having energies above a few keV (McEwen et al., 1981; Yau et al., 1981; also see review by Davidson, 1990). Velocity dispersion has demonstrated that in many cases the modulation occurs in the vicinity of the equator (Bryant et al., 1975), and pulsations have been noted in the hiss and chorus emissions there (Gough et al., 1981).

However, other reports of correlations between VLF whistlers and optical emissions (Helliwiell et al., 1980) indicate that the wave scattering of the high energy electrons occurs in a region along the flux tube far from the equator. VLF chorus (Johnstone, 1983), electrostatic electron waves (Lyons, 1974; Gough et al., 1982; Fennell et al., 1991) and whistler mode chorus (Inan et al., 1992) have been presented as agents responsible for causing the scattering of the electrons into the loss cone resulting in their precipitation. A mechanism such as the relaxation oscillator (Davidson, 1979) is then required to modulate the precipitation.

The Pulsating Aurora (PULSAUR) rocket campaign was funded by the Norwegian Space Center to study several outstanding questions regarding pulsating auroras. Typical of these are:

(1) Are the spatial and temporal structures phonomenologically related? What are the coherence scales of the pulsating patches.

(2) Are there underlying relationships that might connect auroral pulsations to energetic radiation belt and high latitude dayside electron precipitation phenomena, such as electron microbursts and relativistic electron precipitation.

(3) What is the role of magnetospheric plasma in promoting auroral pulsations and determining the structure of pulsating patches.

(4) What is the relationship between pulsations causally related to the low-energy vs the high-energy particle populations.

(5) What is the role played by the ionosphere in the processes producing or influencing pulsations.

It was felt that these and perhaps other questions could be answered by flying a suitably instrumented payload over a pulsating auroral event and coordinating the rocket flight with comprehensive ground observations from the launch site and nearby radar sites.

Southwest Research Institute (SwRI) successfully proposed to NASA, through a NASA Research Announcement of Opportunity, to build the electron detector for the second Pulsating Aurora (PULSAUR II). The detector, a tophat analyzer, was to be built by the combined efforts of Southwest Research Institute, NASA's Goddard Space Flight Center (GSFC), the Mullard Space Science Laboratory (MSSL), and the Rutherford Appleton Laboratory (RAL). The instrument was part of a payload containing optical photometers, high-energy particle spectrometers, an X-ray imager, a plasma probe, a magnetometer, and electric field and waves instruments.

PULSAUR LOW-ENERGY ELECTRON SPECTROMETER

The PULSAUR II electron spectrometer is a 360° symmetric quadraspheric energy analyzer based on similar electron spectrometers flown on the Polar ARCS auroral payload (Sharber et al., 1988) and currently being built to fly on CASSINI (Coates et al., 1992). A drawing of the instrument is shown in Figure 1 and photographic views are shown in Figure 2.

For the PULSAUR II mission, the instrument makes differential measurements of electrons in the energy range of 10 eV to 20 keV in 32 energy steps with an energy resolution of 26 %. The particle sensing element is a set of two microchannel plates arranged as a cheveron pair above twenty-four 15° anode segments equally spaced around an annulus. The angular field-of-view corresponding to each segment is 15° x 19°, and the geometric factor for each is 3.3×10^{-3} cm^2 sr. To increase the time resolution of the instrument, the 32 steps are interleaved in the voltage stepping sequence to produce two 16 point spectra. The sweep time for the 16 steps allows a pitch angle distribution with non-contiguous energy resolution to be obtained in 120 ms. The full resolution energy spectrum is measured in 240 ms.

A particle correlator, provided by the University of Sussex, is included in the electron instrument to investigate wave-particle interactions.

A functional diagram of the tophat sensor and processing electronics, the correlator, and the power unit is shown in Figure 3.

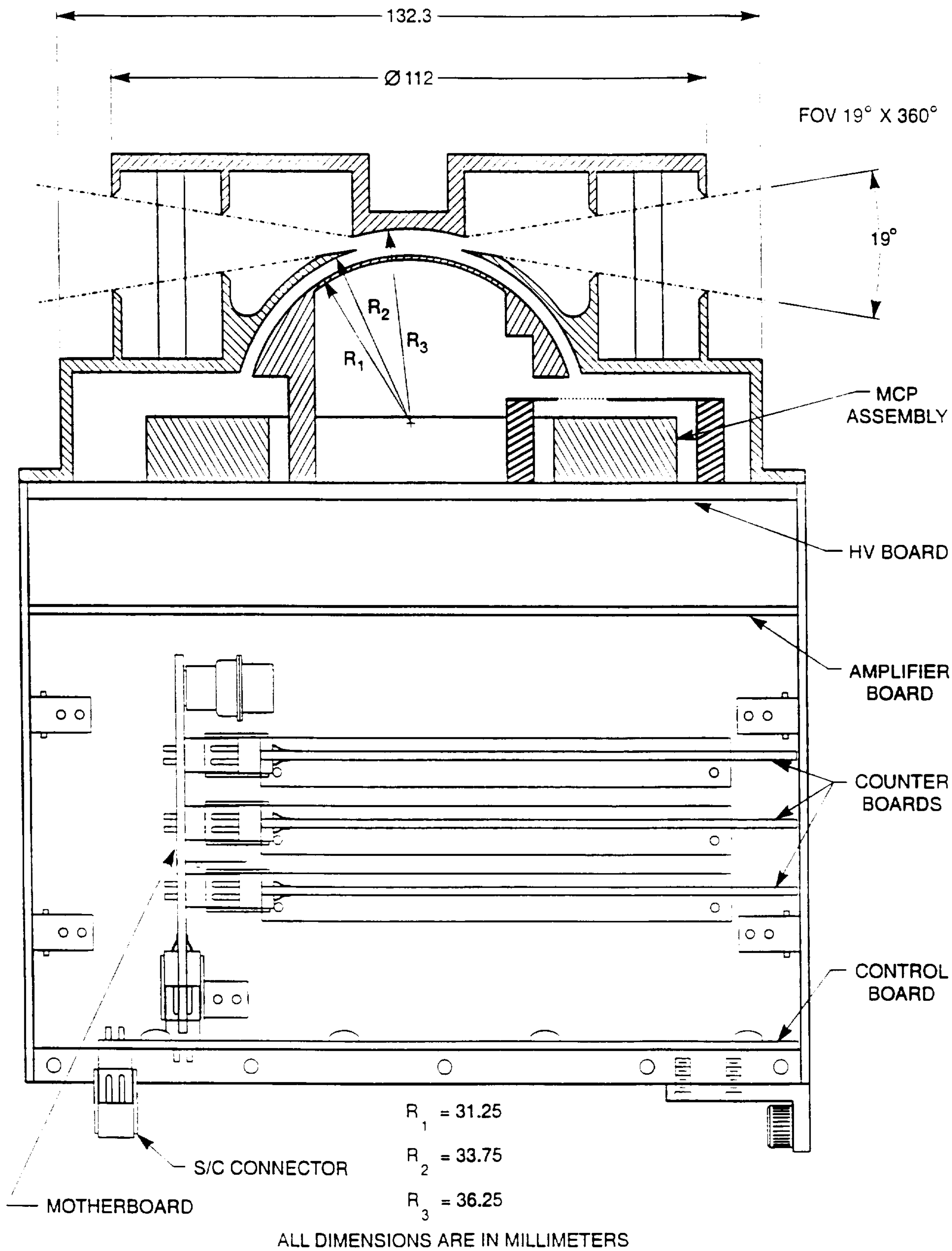

Figure 1. Cross sectional view of the PULSAUR II electron spectrometer. The analyzer portion is a tophat energy per unit charge analyzer. It is cylindrically symmetric about a vertical axis through the center and provides a 19° × 360° field-of-view made up of 24 15°-anode segments. Below the deflection system, the microchannel plate (MCP) assembly and processing circuitry are shown.

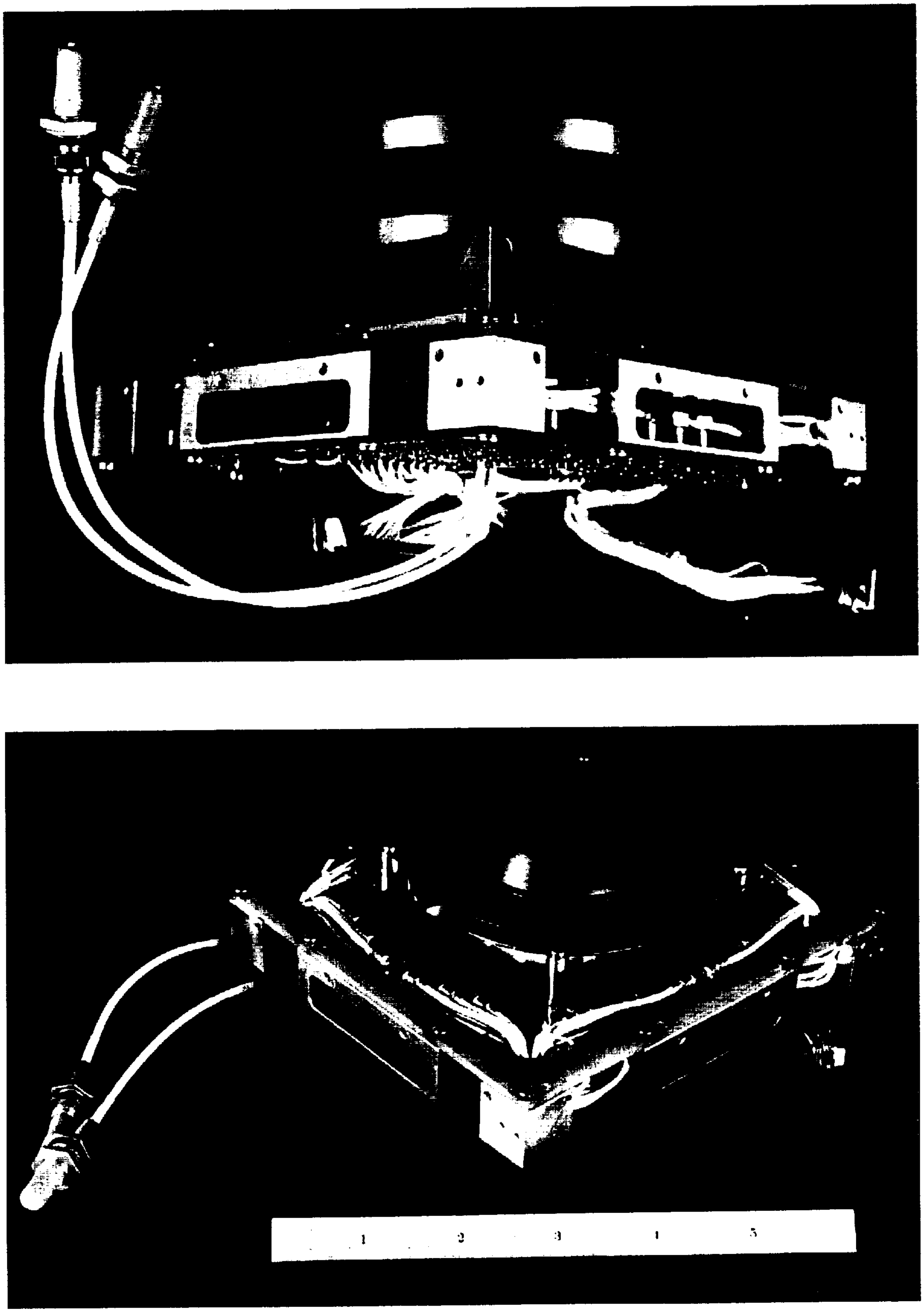

Figure 2. Views of the PULSAUR II Electron Spectrometer.

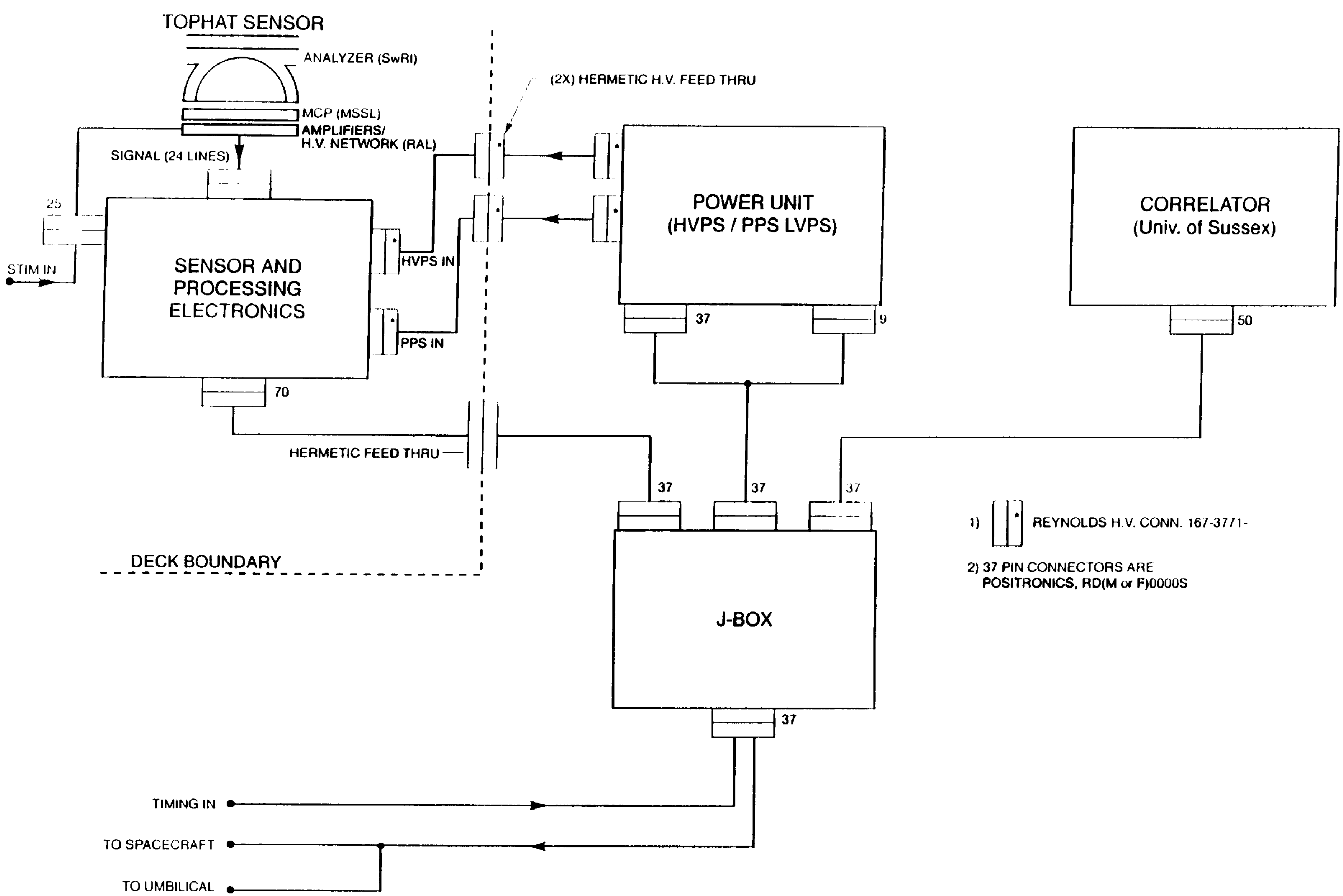

Figure 3. Functional diagram of PULSAUR II Electron Spectrometer Package.

HIGH VOLTAGE POWER SUPPLIES

The high voltage supply for biasing the MCP configuration is derived from a resonant square wave converter, with linear control, producing 2700 volts DC. Feedback from the output is compared against a precision reference to provide regulation of the output against line, load, and temperature. A monitor scales the output by 555 (2700 volts = 4.865 volts).

A programmable high voltage supply for deflection is also included. This stepping supply is controlled by a 12 bit D/A converter. Feedback from the output is compared against the analog output of the converter for precision control of the deflection voltage. The stepping supply topology is similar to that of the MCP supply. The monitor scaling is output divided by 700 (3252 volts = 4.646 volts). The programmable power supply steps the inner deflection plate through 32 voltage steps logarithmically spaced between 9.252 and 19,941 V. The values of voltage at each step and the corresponding center energies are shown in Table 1. The Power Unit, containing the two high voltage supplies and the +5 V regulated supply, is shown in Figure 4.

CALIBRATION

The PULSAUR electron tophat calibration consisted of making detailed measurements of energy and angular resolution at various anodes around the circular anode pattern. In addition, in order to determine the relative throughput factor of each of the 24 anodes, relative responses from each channel were measured. This was done by peaking the count in each channel in energy, theta, and phi for a given potential difference between the tophat plates.

The calibration measurements yielded results that compared very favorably with the simulation results of the MSSL group (Woodliffe, 1991). The measured values for the anodes calibrated are shown in Table 2. The average values for the deflection constant (K) and energy resolution ($\Delta E/E$) are 6.16 eV/V and 25.7%, respectively. The laboratory data for the four anodes taken through complete calibration runs are shown in Figure 5, which shows the three standard values (the median, the mean, and the most probable) of the energy resolution and deflection constant. These measured values were averaged to obtain the values ascribed to each anode. Angular responses for the same four anodes for the polar angle, ϕ, are shown in Figure 6. This response lies in the plane normal to the anode surface containing a line drawn radially from the central axis of the spectrometer. The average value of the FWHM angular responses is $\Delta\phi = 10.1°$.

Table 1. Voltage Levels and Center Energies

Step Number	Voltage Level (V)	Center Energy (eV)
0	3237.2	19941
1	3234.2	19923
2	1988.0	12246
3	1219.2	7510
4	744.7	4587
5	456.5	2812
6	279.3	1720
7	170.2	1048
8	104.1	643.1
9	64.06	394.6
10	39.54	243.6
11	23.62	145.5
12	14.91	91.85
13	8.509	52.41
14	5.405	33.29
15	3.103	20.96
16	2.302	14.18
17	2536.5	15625
18	1556.5	9588
19	953.0	5870
20	583.6	3595
21	357.4	2202
22	218.2	1344
23	134.1	826.3
24	82.08	505.6
25	50.05	308.3
26	30.73	189.3
27	18.92	116.5
28	11.71	72.13
29	7.007	43.16
30	3.904	24.05
31	2.302	14.18
32	1.502	9.252

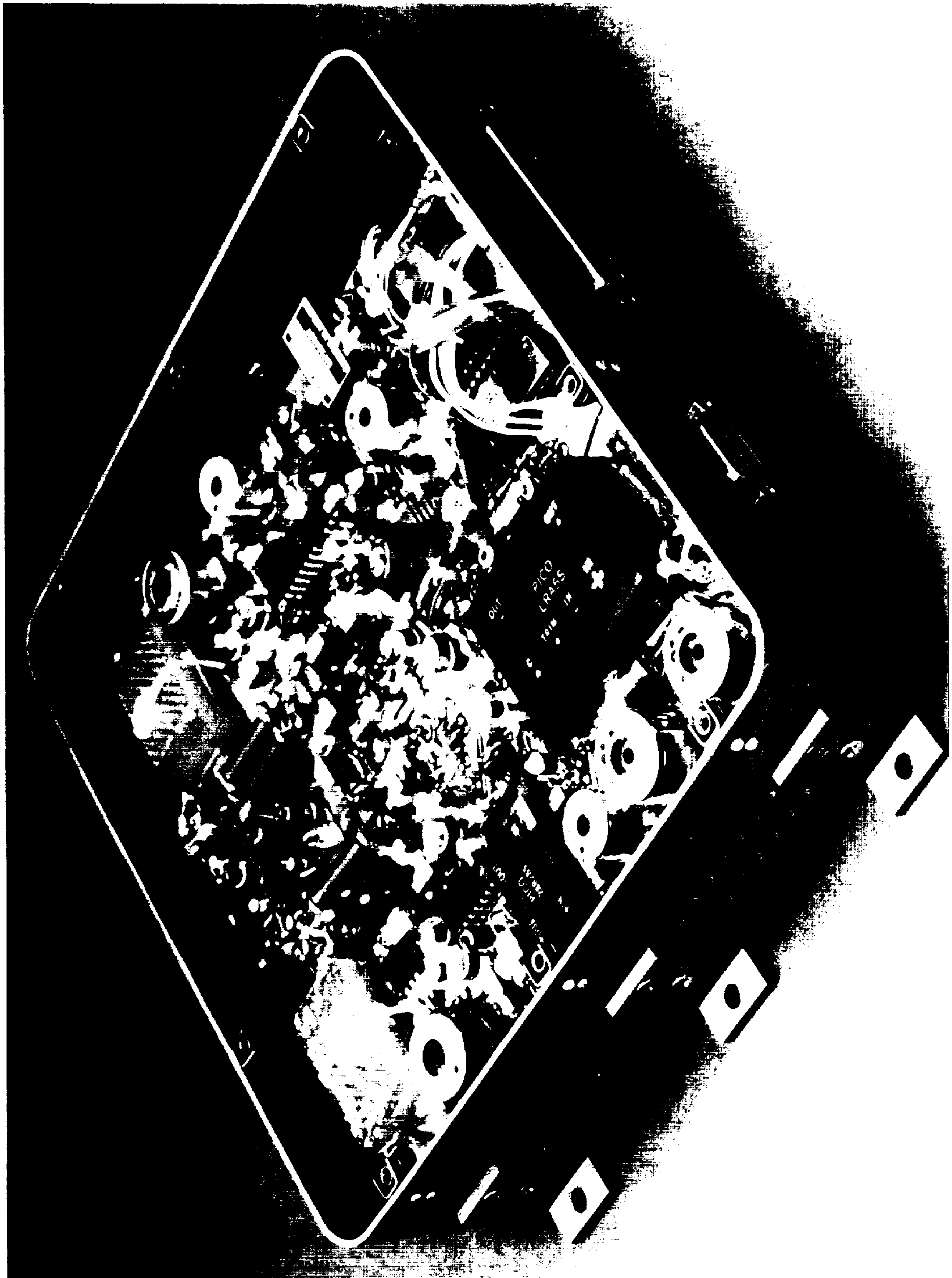

Figure 4. **PULSAUR II electron spectrometer Power Unit containing the high-voltage biasing supply and the programmable stepping supply.**

ERGY INTEGRATION

INSTRUMENT: 1-23

Voltage = 1000.000

Plot # 1765.000
Date Recorded: 93210
Date Processed: 03-AUG-93
Theta = 0.000

Only graph data points used for these calculations:
data integral: 1530546805.120

Arithmetic mean calculations
CR: 837270.055
ELECTRON BEAM ENERGY : 6151.453
ELECTRON BEAM ENERGY l: 5186.288
Sensitivity: 6.151

CR/2: 418635.027
FWHM: 1667.953
ELECTRON BEAM ENERGY u: 6854.242
Resolution: 0.271

Median calculations
CR: 880288.376
ELECTRON BEAM ENERGY : 6056.781
ELECTRON BEAM ENERGY l: 5204.190
Sensitivity: 6.057

CR/2: 440144.188
FWHM: 1609.993
ELECTRON BEAM ENERGY u: 6814.183
Resolution: 0.266

Most probable value calculations
CR: 927314.000
ELECTRON BEAM ENERGY : 5896.430
ELECTRON BEAM ENERGY l: 5223.879
Sensitivity: 5.896

CR/2: 463657.000
FWHM: 1548.234
ELECTRON BEAM ENERGY u: 6772.113
Resolution: 0.263

All data points used for these calculations:
data integral: 1598841321.080

Arithmetic mean calculations
CR: 837608.699
ELECTRON BEAM ENERGY : 6150.749
ELECTRON BEAM ENERGY l: 5186.430
Sensitivity: 6.151

CR/2: 418804.349
FWHM: 1667.491
ELECTRON BEAM ENERGY u: 6853.921
Resolution: 0.271

Median calculations
CR: 881882.208
ELECTRON BEAM ENERGY : 6052.980
ELECTRON BEAM ENERGY l: 5204.854
Sensitivity: 6.053

CR/2: 440941.104
FWHM: 1607.874
ELECTRON BEAM ENERGY u: 6812.728
Resolution: 0.266

Most probable value calculations
CR: 927314.000
ELECTRON BEAM ENERGY : 5896.430
ELECTRON BEAM ENERGY l: 5223.877
Sensitivity: 5.896

CR/2: 463657.000
FWHM: 1548.236
ELECTRON BEAM ENERGY u: 6772.113
Resolution: 0.263

e and Deflection Constant for Anode 23. Shown on the graph are obable, arithmetic mean, and median. Numerical values are shown

ELECTRON BEAM ENERGY INTEGRATION

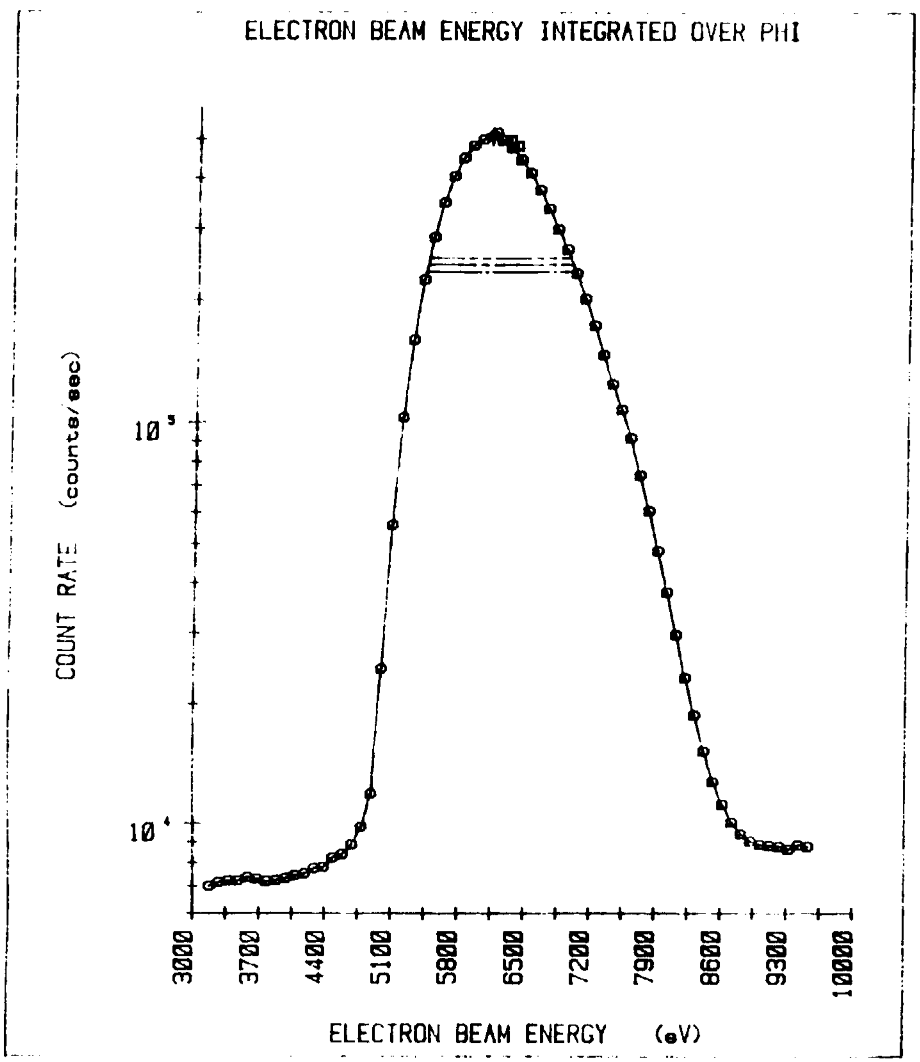

INSTRUMENT: 1-13

Voltage = 1000.000

Plot # 1975.000
Date Recorded: 93210
Date Processed: 17-JAN-96
Theta = 0.000

Only graph data points used for these calculations:
data Integral: 835254595.296

Arithmetic mean calculations

CR: 470517.824	CR/2: 235258.912
ELECTRON BEAM ENERGY : 6318.985	FWHM: 1590.544
ELECTRON BEAM ENERGY l: 5408.987	ELECTRON BEAM ENERGY u: 6999.532
Sensitivity: 6.319	Resolution: 0.252

Median calculations

CR: 489573.471	CR/2: 244786.735
ELECTRON BEAM ENERGY : 6239.268	FWHM: 1546.469
ELECTRON BEAM ENERGY l: 5424.664	ELECTRON BEAM ENERGY u: 6971.133
Sensitivity: 6.239	Resolution: 0.248

Most probable value calculations

CR: 511978.000	CR/2: 255989.000
ELECTRON BEAM ENERGY : 6098.010	FWHM: 1494.670
ELECTRON BEAM ENERGY l: 5443.344	ELECTRON BEAM ENERGY u: 6938.014
Sensitivity: 6.098	Resolution: 0.245

Figure 5(b). Same as Figure 5(a) except for Anode 13.

ELECTRON BEAM ENERGY INTEGRATION

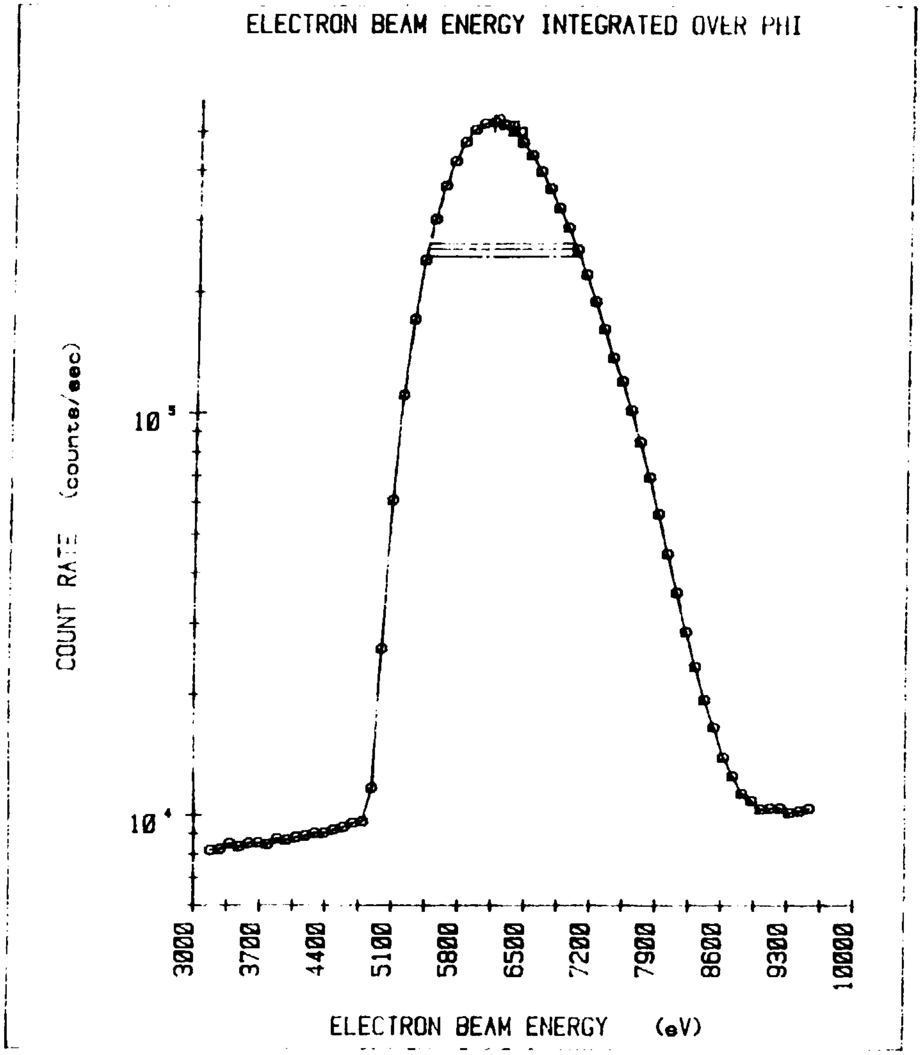

INSTRUMENT: 1-12

Voltage = 1000.000

Plot # 1892.000
Date Recorded: 93210
Date Processed: 17-JAN-96
Theta = 0.000

Only graph data points used for these calculations:
data integral: 893931574.561

Arithmetic mean calculations
CR: 491090.907
ELECTRON BEAM ENERGY : 6334.315
ELECTRON BEAM ENERGY l: 5400.775
Sensitivity: 6.334
CR/2: 245545.454
FWHM: 1633.140
ELECTRON BEAM ENERGY u: 7033.915
Resolution: 0.258

Median calculations
CR: 511097.871
ELECTRON BEAM ENERGY : 6252.525
ELECTRON BEAM ENERGY l: 5416.597
Sensitivity: 6.253
CR/2: 255548.936
FWHM: 1587.248
ELECTRON BEAM ENERGY u: 7003.815
Resolution: 0.254

Most probable value calculations
CR: 530493.000
ELECTRON BEAM ENERGY : 6098.010
ELECTRON BEAM ENERGY l: 5432.238
Sensitivity: 6.098
CR/2: 265246.500
FWHM: 1542.559
ELECTRON BEAM ENERGY u: 6974.797
Resolution: 0.253

Figure 5(c). Same as Figure 5(a) except for Anode 12.

ELECTRON BEAM ENERGY INTEGRATION

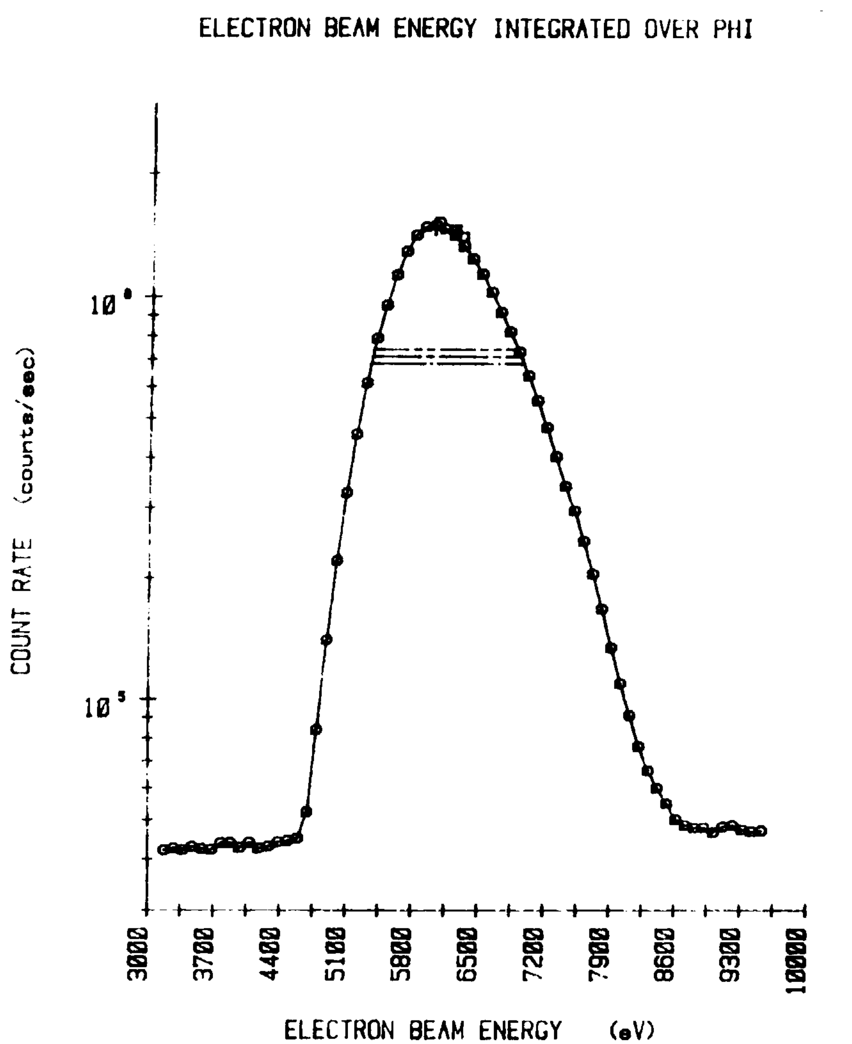

INSTRUMENT: 1-1

Voltage = 1000.000

Plot # 1888.000
Date Recorded: 93209
Date Processed: 17-JAN-96
Theta = 0.000

Only graph data points used for these calculations:
data integral: 2569320838.010

Arithmetic mean calculations
CR: 1372574.438
ELECTRON BEAM ENERGY : 6245.147
ELECTRON BEAM ENERGY l: 5332.907
Sensitivity: 6.245

CR/2: 686287.219
FWHM: 1622.622
ELECTRON BEAM ENERGY u: 6955.529
Resolution: 0.260

Median calculations
CR: 1428711.461
ELECTRON BEAM ENERGY : 6162.995
ELECTRON BEAM ENERGY l: 5348.555
Sensitivity: 6.163

CR/2: 714355.730
FWHM: 1576.321
ELECTRON BEAM ENERGY u: 6924.876
Resolution: 0.256

Most probable value calculations
CR: 1492028.000
ELECTRON BEAM ENERGY : 5997.220
ELECTRON BEAM ENERGY l: 5366.291
Sensitivity: 5.997

CR/2: 746014.000
FWHM: 1523.308
ELECTRON BEAM ENERGY u: 6889.599
Resolution: 0.254

Figure 5(d). Same as Figure 5(a) except for Anode 1.

PHI INTEGRATION

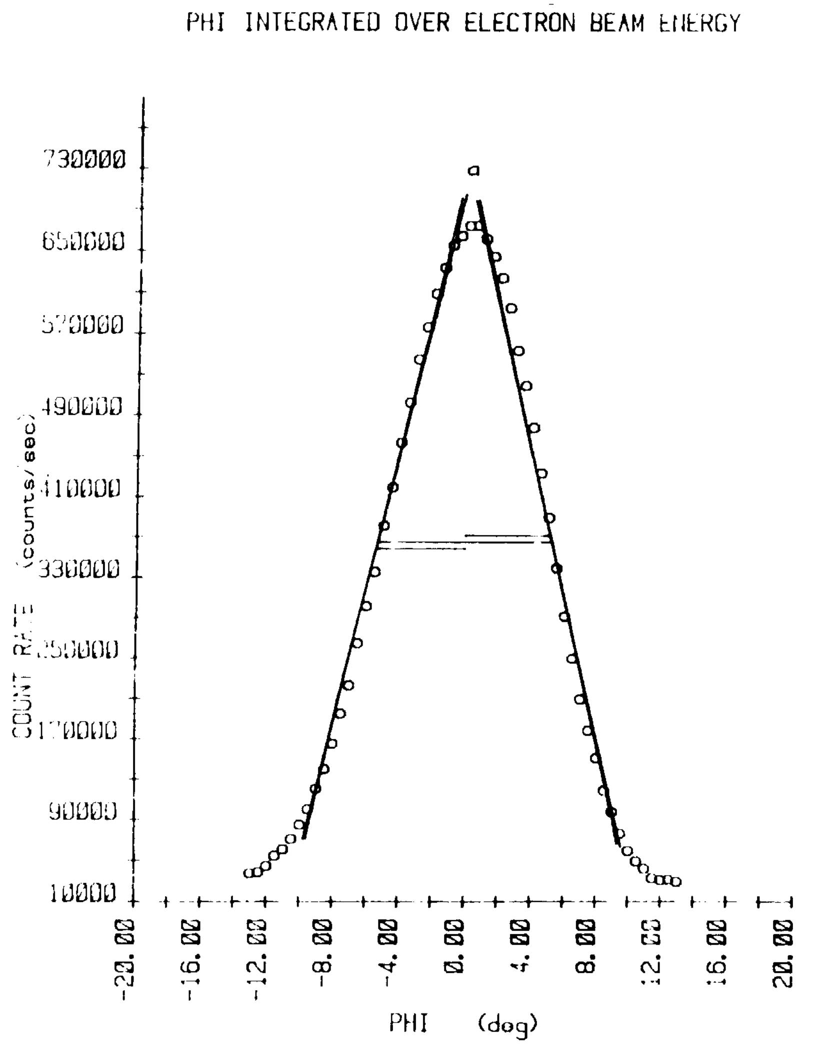

INSTRUMENT: 1-23

Voltage = 1000.00

Plot # 1766.00
Date Recorded: 93210
Date Processed: 03-AUG-93
Theta = 0.00

Only graph data points used for these calculations:

Single least squares line calculations
Y = (-68996.60)X + (725649.54)   Coeff. of determination: 0.99
Data integral: 7627452.19   Line integral: 5797620.38
FWHM: 10.58   PHI peak: -0.06   CR: 729827.07
PHI l: -5.35   PHI u: 5.23   CR/2: 364913.54
Arithmetic mean: -0.15

Split least squares calculations
left line calculations:
Y = (66499.50)X + (720395.83)   Coeff. of determination: 0.99
Data integral: 3501574.40   Line integral: 3029629.02
HWHM: -5.39   PHI peak: -0.06   CR: 716369.49
PHI l: -5.45   PHI u: -0.06   CR/2: 358184.75
right line calculations:
Y = (-71897.92)X + (739299.31)   Coeff. of determination: 0.98
Data integral: 3791526.30   Line integral: 2803341.67
HWHM: 5.17   PHI peak: -0.06   CR: 743652.51
PHI l: -0.06   PHI u: 5.11   CR/2: 371826.25

Figure 6(a). Angular Response in Phi for Anode 23. The response is measured in the plane containing the instrument axis of symmetry and the peak response point of Anode 23.

PHI INTEGRATION

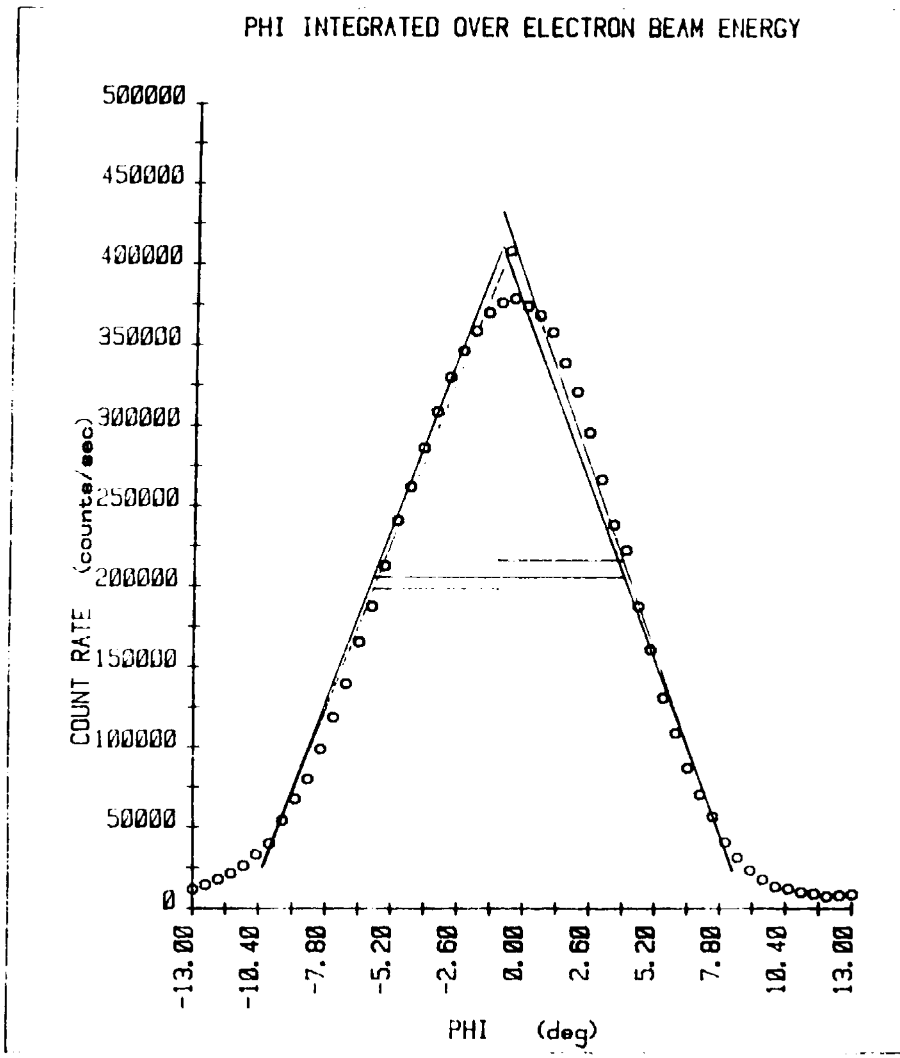

INSTRUMENT: 1-13

Voltage = 1000.00

Plot # 1977.00
Date Recorded: 93210
Date Processed: 17-JAN-96
Theta = 0.00

Only graph data points used for these calculations:

Single least squares line calculations
Y = (-41580.83)X + (369531.14) Coeff. of determination: 0.98
Data integral: 4035572.13 Line integral: 3585304.46
FWHM: 9.89 PHI peak: -1.00 CR: 411111.97
PHI 1: -5.94 PHI u: 3.94 CR/2: 205555.99
Arithmetic mean: 0.87

Split least squares calculations
left line calculations:
Y = (40229.38)X + (437469.49) Coeff. of determination: 0.99
Data integral: 1746254.13 Line integral: 1722156.29
HWHM: -4.94 PHI peak: -1.00 CR: 397240.11
PHI 1: -5.94 PHI u: -1.00 CR/2: 198620.05
right line calculations:
Y = (-44146.93)X + (388769.77) Coeff. of determination: 0.99
Data integral: 1913536.45 Line integral: 1884553.53
HWHM: 4.90 PHI peak: -1.00 CR: 432916.70
PHI 1: -1.00 PHI u: 3.90 CR/2: 216458.35

Figure 6(b). Angular Response in Phi for Anode 13.

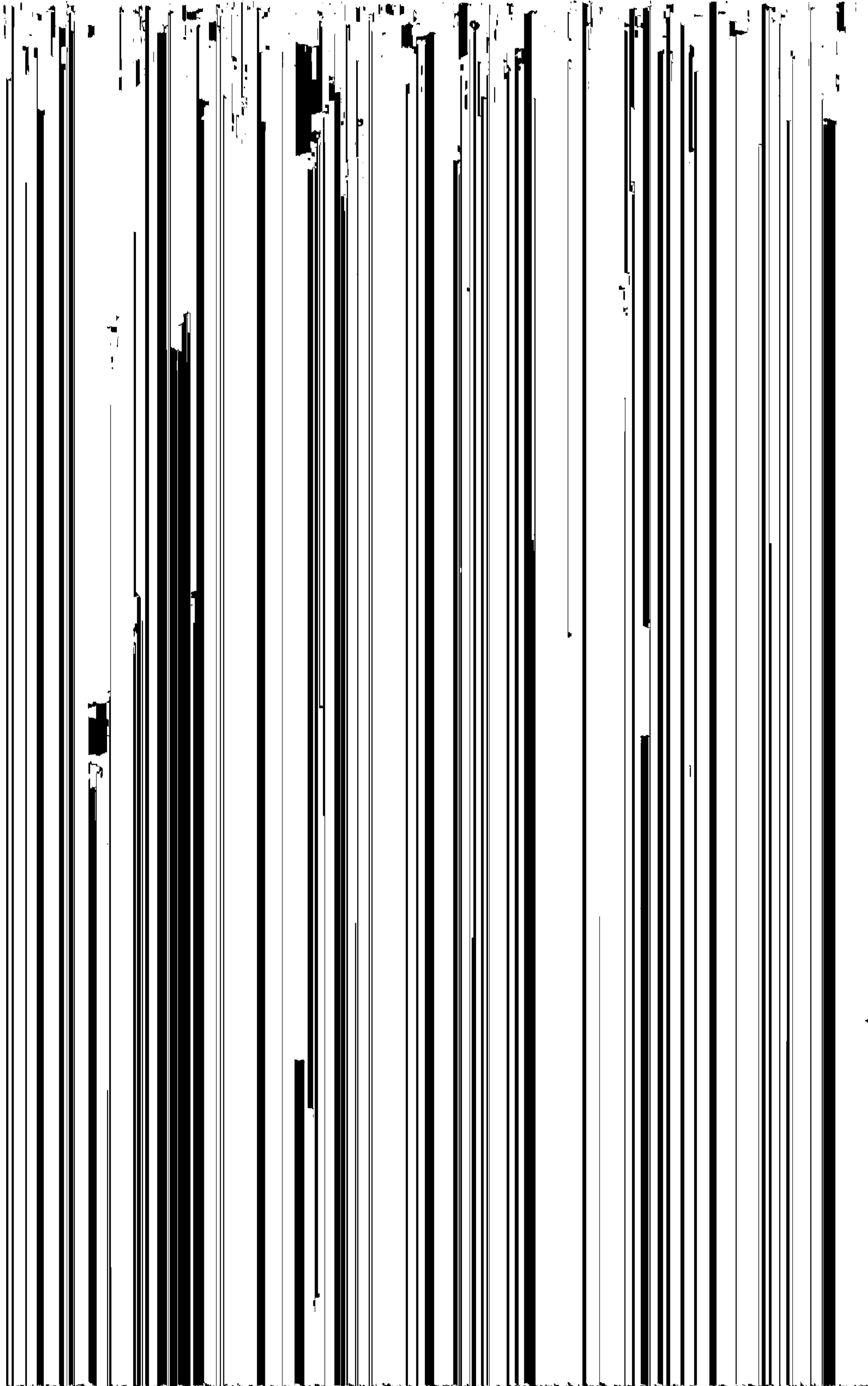

```
N

ENT: 1-12                                  Plot #  1894.00
                                           Date Recorded:   93210
                                           Date Processed:   17-JAN-96
 =  1000.00                                Theta =  0.00

aph data points used for these calculations:

least squares line calculations
7027.68)X + ( 778615.99)          Coeff. of determination:   0.98
tegral:  8667121.54             Line integral:   7769030.25
10.02              PHI peak:  -1.08           CR:   872272.74
-6.09              PHI u:   3.94              CR/2:   436136.37
tic mean:  -1.15

east squares calculations
 left line calculations:
3029.78)X + ( 940048.41)          Coeff. of determination:   0.99
tegral:  3957457.31             Line integral:   3860727.19
5.12               PHI peak:  -1.08           CR:   850694.09
-6.20              PHI u:  -1.08              CR/2:   425347.05
right line calculations:
(664.79)X + ( 795894.55)          Coeff. of determination:   0.98
tegral:  4305911.26             Line integral:   3890504.36
1.88               PHI peak:  -1.08           CR:   894541.62
-1.08              PHI u:   3.80              CR/2:   447270.81
```

e in Phi for Anode 12.

PHI INTEGRATION

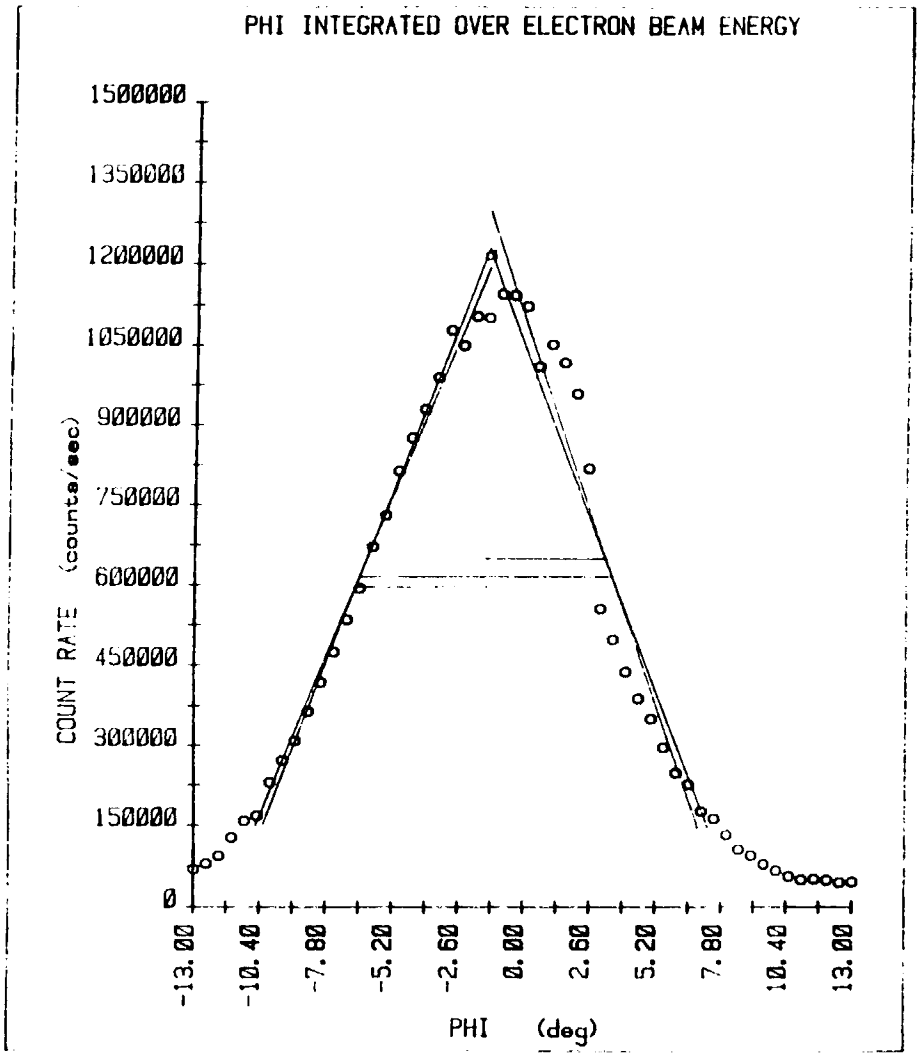

INSTRUMENT: 1-1

Voltage = 1000.00

Plot # 1891.00
Date Recorded: 93209
Date Processed: 17-JAN-96
Theta = 0.00

Only graph data points used for these calculations:

Single least squares line calculations
Y = (-123220.39)X + (1043658.90)   Coeff. of determination: 0.96
Data integral: [illegible]0.58   Line integral: 9439454.67
FWHM: 9.97   PHI peak: -1.50   CR: 1228489.49
PHI l: -6.48   PHI u: 3.48   CR/2: 614244.75
Arithmetic mean: -1.66

Split least squares calculations
left line calculations:
Y = (115122.11)X + (1366620.11)   Coeff. of determination: 0.99
Data integral: 5475515.87   Line integral: 4733245.68
HWHM: -5.19   PHI peak: -1.50   CR: 1193936.95
PHI l: -6.69   PHI u: -1.50   CR/2: 596968.4[illegible]
right line calculations:
Y = (-137958.74)X + (1092341.97)   Coeff. of determination: 0.9[illegible]
Data integral: 5469793.99   Line integral: 4787023.50
HWHM: 4.71   PHI peak: -1.50   CR: 1299280.08
PHI l: -1.50   PHI u: 3.21   CR/2: 649640.01

Figure 6(d). Angular Response in Phi for Anode 1.

Table 2. Calibration Results

Anode	K (eV/V)	ΔE/E (eV/eV)	Δϕ (deg)
1-1	6.141	0.257	9.96
1-12	6.228	0.255	10.0
1-13	6.219	0.248	9.84
1-23	6.035	0.267	10.6
Average	6.156	0.257	10.1

Based on laboratory testing and calibration, Many anodes contained noise in excess of our expectations with noise levels between 30 and 2000 counts/sec. The latter value is an extreme case, but most values were in the low hundreds. Also note that the noise count/sec is to be divided by 200 to obtain the count/accumulation period in the experiment. So a noise count rate of 2000 counts/sec corresponds to a count per accumulation period of only 5 counts. Noise counts were recorded for all anodes at deflection voltages of 0, 1000, 2000, and 3000 V in order to be able to determine noise background levels for data analysis.

Instrumental characteristics based on the calibration results and instrument physical parameters are provided in the following table.

Table 3. Instrumental Characteristics

Instrument type: tophat analyzer

Deflection plate sizes (cm) : r_1, r_2. r_3 = 3.125, 3.375, 3.625

Energy resolution ΔE/ E = 25.7%

Deflection constant K = 6.16 (lab data)

Angular sectors: 15° x 19° (each sector)

Full FOV: 360° x 19° (There are 24 of the 15° sectors around 360°)

Geometric Factor: G = 3.3 x 10^{-3} cm^2 sr

(Geometric factor is determined by modeling of the instrument by M. Sablik of SwRI and R. Woodliffe of MSSL.)

The differential number flux [#/cm^2 s sr eV] is computed by

$$j(E) = C(E)/ G \Delta E \Delta t \eta(E)$$

where C(E) is the number of counts accumulated in time Δt at energy E, and $\eta(E)$ is the instrument detection efficiency.

$$j(E) = 4.25 \times 10^5 C(E) / E$$

where the energy is in eV. This last expression assumes a detection efficiency for electrons of 0.5.

THE PULSAUR II FLIGHT

The campaign, featuring the instrumented payload and well-coordinated ground-based observations, culminated in the successful launch of a Black Brant IX rocket into a bright, active pulsating aurora at 2343:00 UT on February 9, 1994. The flight took place during the recovery phase of a magnetic substorm. The payload contained photometers, high and low-energy particle detectors, electric and magnetic field experiments, and an X-ray detector. Ground observatory instrumentation included auroral line photometers, all-sky TV, a riometer, a magnetometer, an ionosonde a VLF receiver, and the EISCAT radar.

Electron Spectrometer Data

An example of flight data from the electron spectrometer is shown in Figure 7. The panel shows an energy-time spectrogram from sensor 0 (one of the 24 anodes in the acceptance plane) between T+ 118 s to T+ 358 s. The structures between about 127 s and 300 s are auroral inverted V structures with peak energies in the few hundred eV to 2 keV range. These structures are currently being investiated by researchers at the University of Bergen, as it appears that some of them are temporal in nature. The same group are also investigating the pulsation events; findings will be reported at the spring AGU meeting (Stadsnes et al., 1996). In Figure 8 we show pulsation data from the AGU paper illustrating the difference in spectral shape over the complete spectrum, which includes the part measured by electron spectrometer (between 10 eV and 20 keV) and that at higher energies (>25 keV) determined from the Unuversity of Bergen on-board high-energy electron detector. Analysis of some of the distinct pulsations have shown dispersion consistent with a source of the pulsations near the magnetic equatorial plane (Stadsnes et al., 1966). This work will be a part of the graduate thesis of Nikolai Ostgaard, a student at the University of Bergen and will also be reported in a publication now in preparation (Ostgaard et al.,1996).

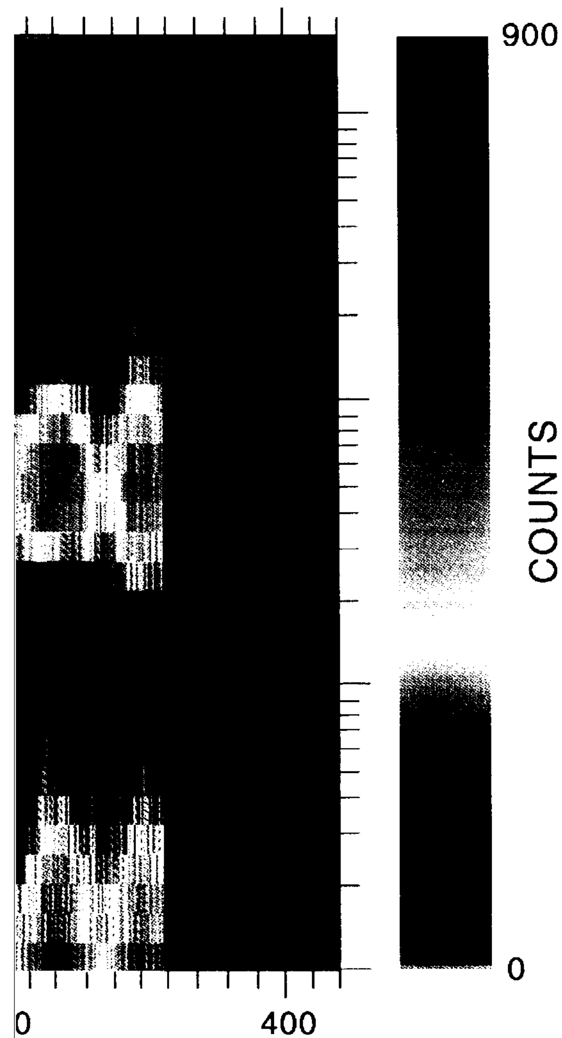

s and T + 358 s . The data are from one of the 24

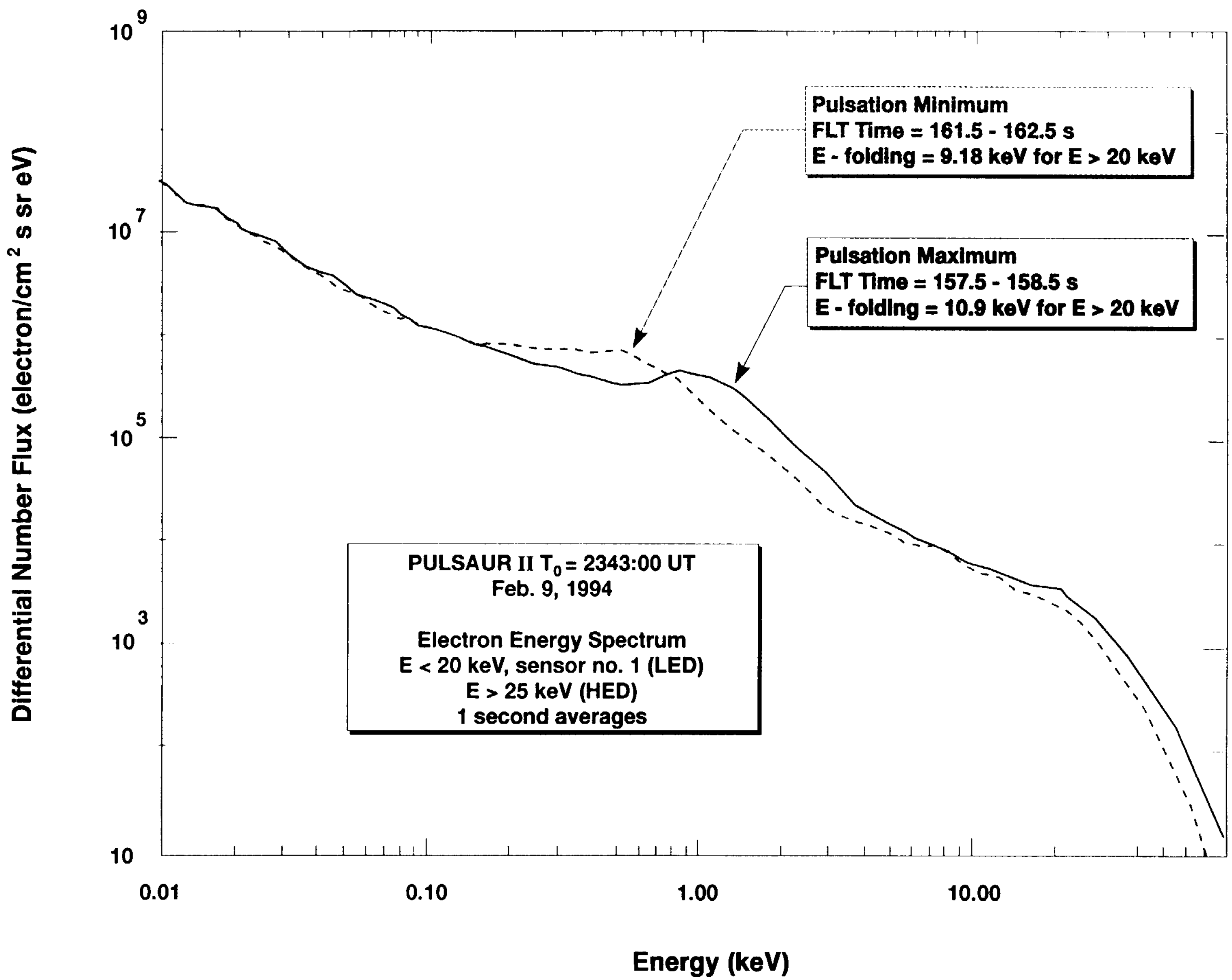

Figure 8. Pulsation maximum and minimum spectra taken from Sensor 1 at T + 162 s and T + 158 s, respectively.

Instrument Performance

This was the first flight of the "Centaur class" tophat; ie, a tophat instrument designed for the CENTAUR rocket investigation of auroral particle and wave observations. Using a microchannel plate on a rocket payload can be risky if the MCP is not kept evacuated until its deployment from the payload. The potential problem is inability of the MCP pores to outgas adequately before high-voltage turn-on. On the PULSAUR II flight, this was the situation.

The high voltage was turned on at T+ 90.3 s (an altitude of 129.3 km). For 29 seconds after high-voltage turn-on, the MCP biasing supply attempted to come up but was intermittant, only sporatically reaching its operating value of 2700 volts. Starting at T+118 s, the high voltage supply became clean at 2700 volts and spectral data were of high quality. This condition lasted until T+358 (an altitude of 321 km), when the supply again became intermittant, reaching the proper operational voltage only sporatically until high-voltage turn-off at T+486 s. The result was that 128 of data were lost on the downleg of the flight.

The payload was not recovered. However, study of the electronics suggests that the transformer in a purchased low-voltage converter within the high-voltage power unit may have failed. Because of the importance of eliminating such occurrence on future flights, we will continue to investigate the possible cause(s) of its failure.

PUBLICATIONS AND PRESENTATIONS

The following papers have been presented at AGU meetings or are in preparation for publication. Preprints of submitted papers will be sent to the project office when they are submitted.

(1) "Pulsating Aurora as Observed by the PULSAUR II Sounding Rocket: An Overview," F. Soraas, J. Stadsnes, K. Aarsnes, Bjordal, K. Maseide, J.A. Holtet, M. Smith, R. Pfaff, W. Farrell, J.R. Sharber, M. Grande, presented at the Fall Meeting of the AGU, abstract: EOS, Fall Meeting Supplement, p. F508, 1995.

CONCLUDING COMMENTS

The primary objective of this grant was to provide a low-energy electron spectrometer to be flown on the PULSAUR II rocket payload for investigation of the pulsating aurora. The instrument, a tophat analyser, was built and calibrated by the combined efforts of Southwest Research Institute

Mullard Space Sciences Laboratory, the Rutherford Appleton Laboratory, and Goddard Space Flight Center. It was successfully flown into an active, early morning, pulsating aurora over Andoya, Norway, on February 9, 1994. The high-time resolution data obtained by the spectrometer during the flight is currently being used in several studies of auroral pulsations. Tentative results support a pulsation source near the midnight sector magnetic equator.

REFERENCES

Bryant, D. A., M. J. Smith, and G. M. Courtier, "Distant modulation of electron intensity during the expansion phase of an auroral substorm", *Planet Space Sci.*, **23**, 867, 1975.

Coates, A. D., C. Alsop, A. J. Coker, D. R. Linder, A. D. Johnstone, R. D. Woodliffe, M. Grande, A. Preece, S. Burge, D. S. Hall, B. Narheim, K. Svenes, D. T. Young, J. R. Sharber, and J. R. Scherrer, J. British Interplanetary Soc., 45, 387, 1992.

Davidson, Gerald T., "Pitch angle diffusion and the origin of temporal and spatial structures in morningside aurora", *Space Sci. Rev.*, **53**, 45-82, 1990.

Davidson, G. T., "Self modulation of VLF wave-electron interactions in the magnetosphere: a cause of auroral pulsations", *J. Geophys. Res.*, **84**, 6517, 1979.

Fennell, J. F., J. L. Roeder, and T. F. Alsruhe, "A statistical survey of electron pitch angle

Lyons, L. R., "Electron diffusion driven by magnetospheric electrostatic waves", *J. Geophys. Res.*, **79**, 575-580, 1974.

McEwen, D. J., E. Yee, B. A. Whalen, and A. W. Yau, "Electron energy measurements in pulsating auroras, *Can. J. Phys.*, **59**, 1106-1115, 1982.

Ostgaard, N., J. Stadsnes, K. Aarsnes, F. Soraas, Karl Maseide, M. Smith, J. Sharber, Simultaneous measurements of X-rays and electrons during a pulsating aurora, to be submitted to Annales Geophysicae, 1996.

Sharber, J. R., J. D. Winningham, J. R. Scherrer, M. J. Sablik, C. A. Bargainer, P. A. Jensen, B. J. Mask, N. Eaker, J. C, Biard, Design, Construction, and Laboratory Calibration of the Angle Resolving Energy Analyzer (AREA): A "Top-Hat" Instrument for Auroral Research, IEEE Trans. on Geoscience and Remote Sensing, 26, 474, 1988.

Smith, M. F., F. Soraas, J. Stadsnes, K. Aarsnes, G. B. Haaheim and N. Oestgaard, K. Maseide, K. Svenes, M. Grande, J. R. Sharber, Pulsating Aurora as Observed by the PULSAUR II Sounding Rocket: A Comparison of Particle, X-ray, and Photometer Data, presented at the 1995 Fall Meeting of the AGU, abstract: EOS, Fall Meeting Supplement, p.F508, 1995.

Soraas, F., J. Stadsnes, K. Aarsnes, Bjordal, K. Maseide, J.A. Holtet, M. Smith, R. Pfaff, W. Farrell, J.R. Sharber, M. Grande, Pulsating Aurora as Observed by the PULSAUR II Sounding Rocket: An Overview, EOS, Fall Meeting Supplement, p.F508, 1995.

Stadsnes, J., Nikolai Ostgaard, Finn Soraas, Kjell Aarsnes, M. F. Smith, Electron flux modulations during pulsating aurora, presented at Spring Meeting of the AGU, abstract: EOS, Spring Meeting Supplement, p. S238, 1996.

Woodliffe, Roger David, Design of Space Borne Plasma Analyzers by Computer Simulation, Ph.D. Thesis, University of London, September, 1991.

Yau, A. W., B. A. Whalen, and D. J. McEwen, "Rocket borne measurements of particle pulsation in pulsating aurora", *J. Geophys. Res.*, **86**, 5673, 1982.